Title

Real-time compensation of backlash positional errors in CNC machines by localized feedrate modulation

Journal

The International Journal of Advanced Manufacturing Technology, 119(9-10)

ISSN

0268-3768

Authors

Farouki, Rida T

Swett, Jack R

Publication Date

2022-04-01

DOI

10.1007/s00170-021-08515-z

Peer reviewed

Real–time compensation of backlash positional errors in CNC machines by localized feedrate modulation

Rida T. Farouki and Jack R. Swett
Department of Mechanical and Aerospace Engineering,
University of California, Davis, CA 95616, USA

Abstract

A methodology for analyzing the influence of gear backlash in the axis drive systems of a Cartesian CNC machine on positional accuracy is developed. The approach is based on solving the machine dynamical equations in the context of an angular dead–zone backlash model and an osculating circle approximation of smooth paths in a neighborhood each path turning point, which admit an essentially exact solution for a P controller. This methodology is the basis for schemes to minimize backlash degradation of positional accuracy through feedrate or path geometry modifications, rather than hardware or controller upgrades (that may be expensive or disruptive for CNC machines in continuous production use). As a preliminary demonstration of the methodology, results are presented from the use of smooth feedrate reductions about each path turning point as a means to suppress positional inaccuracies incurred by gear backlash in CNC machine axis drive systems.

Keywords: CNC machine, backlash, machine dynamics, osculating circle, feedrate modulation, position error.

e–mail addresses: farouki@ucdavis.edu. jrswett@ucdavis.edu

1 Introduction

To achieve a desired speed (feedrate) of a cutting tool relative to a workpiece along a specified path, computer numerical control (CNC) machines employ feedback controllers to independently drive each machine axis. Typically, the axes are powered by electric motors driving ball screws through geared speed reducers. Thus, characterizing and compensating for the internal dynamics of these drive systems can be an important consideration [3, 26] in guaranteeing consistently high accuracy in machining complex part shapes.

Such "inverse dynamics" compensation schemes may be based on machine hardware or controller upgrades, but these may often be infeasible, expensive, or disruptive for existing CNC machines employed in continuous production use. An alternative approach is to achieve the compensation by modification of the part programs — i.e., by altering the toolpaths and associated feedrates [4, 17]. This approach can prove effective in compensating for the inertia and damping of the axes, by solving the system differential equations "backwards" to identify the input required to achieve a prescribed output.

An aspect of the axis drive system dynamics that is much more difficult to compensate for than inertia and damping is *backlash* in the axis gear system, since it incurs a discontinuous relation between the commanded and executed motions. For a Cartesian machine, backlash occurs when the path tangent is orthogonal to one machine axis, and the path lies locally on one side of the tangent, implying a reversal in the direction of motion of that axis.[1]

The goal of this study is to develop methods to minimize degradation of path tracking accuracy incurred by backlash in the drive systems of Cartesian multi–axis CNC machines. The intent is to achieve this goal by alteration of the commanded path geometry and/or feedrates, rather than by modification of the machine hardware or controller software, allowing implementation on existing machines with minimal expense, and a high potential for automation by updating the software used to generate the part programs. It is expected that the proposed approach can significantly improve the positional accuracy of inexpensive low–end machines, or machines that have less–sophisticated controllers or have experienced wear due to heavy usage.

Backlash is an inherent limitation of geared drive systems. Among other considerations, it provides accommodation of finite manufacturing tolerances,

[1] No backlash arises in the exceptional case of an inflectional tangent, since there is no reversal in the direction of axis motion.

thermal expansion, and lubrication of gears. Nordin and Gutman [16] provide a comprehensive survey of control methods to compensate for the influence of backlash on the tracking accuracy of drive systems, including elastic effects and systems driven against external loads. Tarng et al. [21] used a simulated annealing algorithm to determine the optimum parameters for minimization of the backlash contour error along circular paths. Ge and Jouaneh [11] have proposed a linearized model of backlash hysteresis, and based on this model Warnecke and Jouaneh [23] developed an open–loop backlash compensation scheme that employs a modification of the commanded feedrate profile in the vicinity of points where backlash occurs. Shi et al. [18] have analyzed the compensation of transient backlash error in closed–loop feed drives.

A simple "dead–zone" model for gear backlash is adopted — wherein, on reversal of the sense of rotation of the drive motor, the gear system output shaft remains stationary while the motor shaft turns through a finite angle $\Delta\theta_m$. This mechanical decoupling is the dominant aspect of backlash — of much greater magnitude than higher–order effects such as the finite rigidity of mechanical components or impact effects as components re–engage. During the dead–zone interval, the motor becomes disengaged from the axis, and its operation is governed by the control input (determined by the axis position error) and the motor inertia and damping. The dead–zone model facilitates simple *a priori* estimation of the time duration of backlash phases.

The methodology developed herein is based on paths defined by analytic curves, rather than piecewise–linear/circular G code approximations. Real–time interpolators for analytic curves have been proposed [2, 9, 14, 19, 24] by many authors, and can accommodate feedrates specified as functions of time, arc length, or curvature [7, 8, 10, 15, 22, 25]. Another advantage of analytic paths is that they admit an exact determination of the *osculating circle* at the path "turning points" where backlash occurs. Within a neighborhood of each point on a general curvilinear path, the osculating circle offers a simple but accurate path approximation, that can be exploited to formulate and analyze backlash compensation schemes based on part program modification.

The plan for the remainder of this paper is as follows. Section 2 proposes use of the osculating circle at the turning points of a smooth analytic path as the basis for backlash compensation, and develops an estimate for the extent over which the osculating circles deviates from the path by no more than a prescribed tolerance ϵ. Section 3 formulates a dynamic model for an axis drive system with backlash, that will be employed to determine the onset and duration of each backlash interval. Section 4 then considers this model

in the context of the osculating circle path approximation — namely, the simple harmonic motion of an axis. As a preliminary backlash compensation scheme, Section 5 consider the use of feedrate suppression in the vicinity of turning points, and Section 6 presents simulation results that demonstrate the efficacy of this approach. Finally, Section 7 summarizes and assesses the results of the present study, and identifies directions for further investigation.

2 Osculating circle approximation

For brevity, only planar paths in the (x, y) plane are considered here, since the extension to spatial paths is straightforward. Along a general curvilinear path, the neighborhood of a point of vertical or horizontal tangent (and non–zero curvature) can be accurately approximated by the path osculating circle at that point. The influence of backlash can thus be accurately assessed by considering the machine dynamics along the local osculating circle, which for a prescribed feedrate corresponds to out–of–phase simple harmonic motion of two orthogonal axes. The osculating circle path approximation forms the basis for development of the backlash compensation schemes.

The *parametric speed* $\sigma(\xi) = |\mathbf{r}'(\xi)| = \sqrt{x'^2(\xi) + y'^2(\xi)}$ of a plane curve $\mathbf{r}(\xi) = (x(\xi), y(\xi))$ defines the derivative $\mathrm{d}s/\mathrm{d}\xi$ of its arc length s with respect to the parameter ξ. Thus, derivatives with respect to ξ and s are related by

$$\frac{\mathrm{d}}{\mathrm{d}s} \;=\; \frac{1}{\sigma(\xi)}\frac{\mathrm{d}}{\mathrm{d}\xi}\,, \tag{1}$$

and will henceforth be indicated by primes and dots, respectively. The unit tangent and normal vectors and the curvature of $\mathbf{r}(\xi)$ are defined by

$$\mathbf{t}(\xi) \;=\; \frac{\mathbf{r}'(\xi)}{|\mathbf{r}'(\xi)|}\,, \quad \mathbf{n}(\xi) \;=\; \mathbf{z} \times \mathbf{t}(\xi)\,, \quad \kappa(\xi) \;=\; \frac{(\mathbf{r}'(\xi) \times \mathbf{r}''(\xi)) \cdot \mathbf{z}}{\sigma^3(\xi)}\,, \tag{2}$$

where $\mathbf{z}$ is a unit vector orthogonal to the (x, y) plane, such that $(\mathbf{t}, \mathbf{n}, \mathbf{z})$ form a right–handed orthonormal frame. The curvature determines the variation of $\mathbf{t}$ and $\mathbf{n}$ through [20] the relations

$$\frac{\mathrm{d}\mathbf{t}}{\mathrm{d}s} \;=\; \kappa\,\mathbf{n}\,, \quad \frac{\mathrm{d}\mathbf{n}}{\mathrm{d}s} \;=\; -\,\kappa\,\mathbf{t}\,.$$

A differentiable curve $\mathbf{r}(\xi)$ can be expanded [20] in a Taylor series in the arc length s measured from a chosen curve point $\mathbf{r}_0 = \mathbf{r}(\xi_0)$ as

$$\begin{aligned}\mathbf{r}(s) \;=\; \mathbf{r}_0 \,+\, \mathbf{t}_0\, s \,+\, \frac{\kappa_0\,\mathbf{n}_0}{2}\, s^2 \,+\, \frac{\dot\kappa_0\,\mathbf{n}_0 - \kappa_0^2\,\mathbf{t}_0}{6}\, s^3 \\ - \frac{3\,\kappa_0\dot\kappa_0\,\mathbf{t}_0 + (\kappa_0^3 - \ddot\kappa_0)\,\mathbf{n}_0}{24}\, s^4 + \cdots\,, \end{aligned} \tag{3}$$

where $\mathbf{t}_0, \mathbf{n}_0$ are the unit tangent and normal vectors, and $\kappa_0, \dot\kappa_0, \ddot\kappa_0$ are the curvature and its first and second arc–length derivatives, all evaluated at ξ_0. Applying the differential operator (1) to the expression in (2), the arc–length derivatives of the curvature can be written [10] as

$$\dot\kappa \;=\; \frac{(\mathbf{r}'\times\mathbf{r}''')\cdot\mathbf{z} - 3\,\sigma^2\sigma'\kappa}{\sigma^4}\,,$$

$$\ddot\kappa \;=\; \frac{(\mathbf{r}''\times\mathbf{r}''' + \mathbf{r}'\times\mathbf{r}'''')\cdot\mathbf{z} - 3\,\sigma(2\,\sigma'^2 + \sigma\sigma'')\kappa - 7\,\sigma^3\sigma'\dot\kappa}{\sigma^5}\,,$$

where the derivatives of the parametric speed $\sigma(\xi)$ are given by

$$\sigma' \;=\; \frac{\mathbf{r}'\cdot\mathbf{r}''}{\sigma}\,, \quad \sigma'' \;=\; \frac{\mathbf{r}'\cdot\mathbf{r}''' + |\mathbf{r}''|^2 - \sigma'^2}{\sigma}\,.$$

Now let $\mathbf{c}(s)$ be the osculating circle at $\mathbf{r}(\xi_0)$, parameterized by arc length s from that point. Since $\mathbf{c}(s)$ agrees with $\mathbf{r}(\xi)$ in position, tangent, normal, and curvature at $\mathbf{r}(\xi_0)$, it is seen from (3) that the deviation $\boldsymbol{\delta}(s) = \mathbf{r}(s) - \mathbf{c}(s)$ is specified by

$$\boldsymbol{\delta}(s) \;=\; \frac{\dot\kappa_0\,\mathbf{n}_0}{6}\, s^3 \;-\; \frac{3\,\kappa_0\dot\kappa_0\,\mathbf{t}_0 - \ddot\kappa_0\,\mathbf{n}_0}{24}\, s^4 + \cdots\,. \tag{4}$$

In general, $\dot\kappa_0 \neq 0$ (i.e., the curvature of $\mathbf{r}(\xi)$ is not an extremum at ξ_0) and the osculating circle has second–order contact with $\mathbf{r}(\xi)$ at that point. The lowest–order deviation between points of corresponding arc length along $\mathbf{c}(s)$ and $\mathbf{r}(s)$ is then identified by the cubic term in (4). However, if $\dot\kappa_0 = 0$ and κ_0 is a local curvature extremum, the osculating circle has third–order contact with the curve. In this case, the deviation (4) reduces to

$$\boldsymbol{\delta}(s) \;=\; \frac{\ddot\kappa_0\,\mathbf{n}_0}{24}\, s^4 + \cdots\,. \tag{5}$$

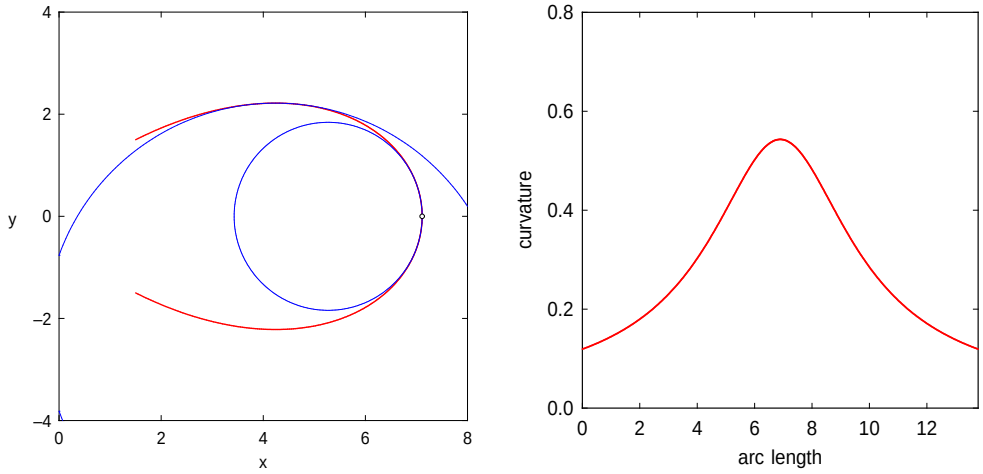

Figure 1: Left: behavior of the osculating circle (blue) for a curve (red) with a horizontal turning point of non–extremum curvature, and a vertical turning point of extremum curvature. Right: the curvature profile for the red curve.

For second–order contact with $\dot{\kappa}_0 \neq 0$, the osculating circle crosses the curve at the point $\mathbf{r}(\xi_0)$. For a third–order contact with $\dot{\kappa}_0 = 0$, on the other hand, the osculating circle lies (locally) to one side of the curve at $\mathbf{r}(\xi_0)$ — some examples of this behavior are illustrated in Figure 1.

Figure 2 illustrates the magnitude of the deviation (4) in the vicinity of vertical and horizontal turning points of the curve in Figure 1. The greater accuracy of the osculating circle at a point of extremum curvature is apparent. Over the range in s shown, the $\mathbf{t}_0$ component of (4) is generally $< 2\%$ of the $\mathbf{n}_0$ component, and can be considered negligible — in fact, as seen in (5), the $\mathbf{t}_0$ component is identically zero for a turning point of extremum curvature.

As a conservative estimate of the maximum arc length s about $\mathbf{r}(\xi_0)$ over which the osculating circle does not deviate from the curve by more than a specified tolerance ϵ, the $\mathbf{t}_0$ term in (4) is omitted to obtain

$$| s | \;=\; \min \left[\, (6\,\epsilon/|\dot{\kappa}_0|)^{1/3}, \, (24\,\epsilon/|\ddot{\kappa}_0|)^{1/4} \, \right] \, . \tag{6}$$

For the curve in Figure 1, the extent defined by (6) is indicated by the dashed lines in Figure 2, with $\epsilon = 10^{-6}$ and $\epsilon = 10^{-5}$ for the vertical and horizontal turning points, respectively — it is evident that (6) is a remarkably accurate estimate. The osculating circles at the vertical and horizontal turning points deviate from the curve by no more than $\epsilon = 10^{-6}$ and $\epsilon = 10^{-5}$ over total arc

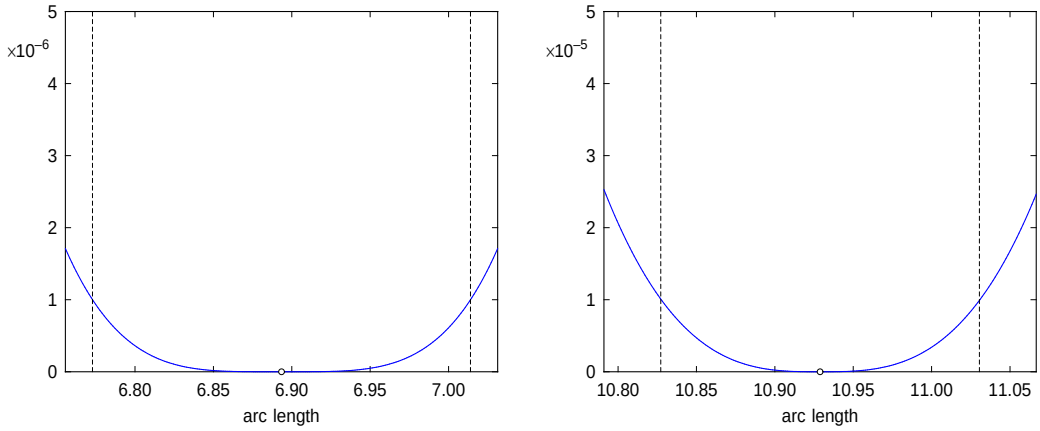

Figure 2: Magnitude of the osculating circle deviation (4) from the curve in Figure 1 in the vicinity of vertical (left) and horizontal (right) turning points — note the different scales in these plots. Dashed vertical lines indicate the extent (6) over which the deviation is less than 10^{-6} (left) and 10^{-5} (right).

lengths $2\,|\,s\,|$ equal to 0.2411 and 0.2033, respectively.

3 Dynamic model formulation

For brevity, only the x–axis dynamics are discussed here: similar principles also apply to the y–axis, with possibly different physical parameters. Figure 3 shows a typical servosystem architecture [1, 26] for a single axis of a CNC machine, comprising a ball screw axis driven through a gearbox by an electric motor governed by a feedback controller.

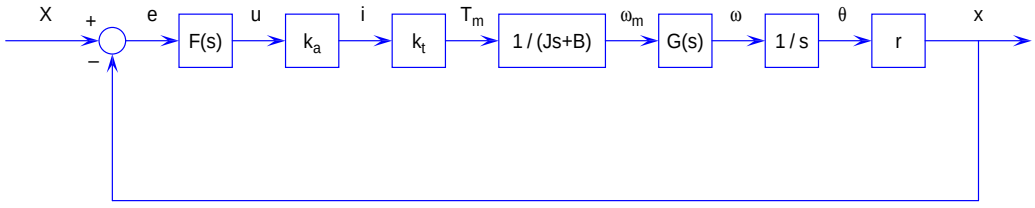

Figure 3: Block diagram for the x–axis drive system dynamics.

In Figure 3, the system variables (and their units) are as follows.

- s (s^{-1}) is the Laplace transform variable;

- $X(s)$, $x(s)$ (m) are Laplace transforms of the commanded and measured axis positions, and $e(s)$ is that of the axis position error;
- $F(s)$ (V/m) is the controller Laplace transfer function;
- u (V) and i (A) are the control voltage and motor current;
- k_a (A/V), k_t (Nm/A) are the current amplifier and motor torque gains;
- J (kg m^2) and B (kg m^2/s) are the overall effective rotary inertia and viscous damping acting on the motor output shaft;
- T_m (Nm) and ω_m (rad/s) are the motor torque and angular speed;
- $G(s)$ (dimensionless) is the Laplace transfer function of the gear system, including backlash;
- ω (rad/s) and θ (rad) are the drive shaft angular speed and position;
- r (m/rad) is the ball screw transmission ratio, i.e., the axis translation for unit rotation of the ball screw.

3.1 Axis drive system

The controller receives the position error $e = X - x$ as input and passes the actuating signal u to the power amplifier, which supplies a current i to the motor. The motor produces a torque T_m that is modulated by the overall system inertia J and damping B to produce a motor speed ω_m that, subject to amplification and backlash of the gear box, yields the angular speed ω of the ball screw drive. Integration of ω then determines the axis linear position x through the transmission ratio r of the ball screw.

For a general PID controller, with transfer function of the form

$$F(s) \;=\; k_p + \frac{k_i}{s} + k_d\, s\,,$$

where k_p, k_i, k_d are the proportional, integral, and derivative gains, the axis equation of motion has — in the absence of backlash — the form

$$a\,\dddot{x} \;+\; b\,\ddot{x} \;+\; c\,\dot{x} \;+\; x \;=\; d\,\ddot{X} \;+\; e\,\dot{X} \;+\; X\,, \tag{7}$$

where dots indicate time derivatives, and the constant coefficients a, b, c, d, e depend on the machine/controller physical parameters, and the cases $k_d = 0$ and $k_i = k_d = 0$ identify PI and P controllers. For brevity (and to facilitate closed–form solutions) the focus here is on a P controller, for which (7) reduces to

$$b\,\ddot{x} + c\,\dot{x} + x = X\,, \tag{8}$$

where, for a gearbox speed reduction ratio N, the coefficients are

$$b = \frac{NJ}{k_p k_a k_t r}\,, \quad c = \frac{NB}{k_p k_a k_t r}\,. \tag{9}$$

These coefficients may be detemined from a system identification procedure. The basic methodology can be extended to PI and PID controllers, although the derivations become more complicated.

3.2 Dead-zone backlash model

To model the backlash, a gearbox transfer function of the form

$$G(s) = \frac{H(s)}{N}$$

is assumed, where $H(s)$ defines the gear backlash, and N is the gear reduction ratio. A simple "dead–zone" model for gear train backlash in the axis drive system is employed. If the motor angular velocity ω_m changes sign at times t_i, a backlash interval Δt_i is associated with each reversal, such that the axis drive shaft angular speed ω satisfies

$$\omega(t) = h(t)\,\omega_m(t)\,, \quad h(t) = \begin{cases} 0 & \text{if} \quad t_i < t \le t_i + \Delta t_i\,, \\ 1 & \text{if} \quad t_i + \Delta t_i < t \le t_{i+1}\,, \end{cases} \tag{10}$$

for each interval i between reversals. Figure 4 gives schematic illustration of the function $h(t)$, which may be expressed as sequence of alternating positive and negative instances of the Heaviside unit step function

$$u(t - t_*) = \begin{cases} 0 & \text{if} \quad t < t_*\,, \\ 1 & \text{if} \quad t > t_*\,. \end{cases}$$

Assuming no backlash at time $t = 0$, the function $h(t)$ can be written as

$$h(t) = u(t) - \sum_i \left[\, u(t - t_i) - u(t - (t_i + \Delta t_i)) \,\right],$$

and its Laplace transform may be expressed as

$$\begin{aligned} H(s) &= \frac{1}{s} - \frac{\mathrm{e}^{-st_1}}{s} + \frac{\mathrm{e}^{-s(t_1+\Delta t_1)}}{s} - \frac{\mathrm{e}^{-st_2}}{s} + \frac{\mathrm{e}^{-s(t_2+\Delta t_2)}}{s} - \cdots \\ &= \frac{1}{s} - \sum_i \frac{\mathrm{e}^{-st_i}}{s}(1 - \mathrm{e}^{-s\Delta t_i})\,. \end{aligned} \tag{11}$$

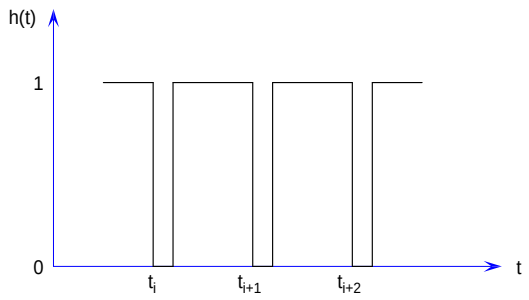

Figure 4: Schematic illustration of the backlash function $h(t)$ defined by (10) relating the drive shaft angular speed ω and motor shaft angular speed ω_m.

In general, the overall inertia J incorporates contributions from the motor internal inertia (J_m), the gear system inertia (J_g), and the axis ball screw drive (J_a), and the overall effective inertia in Figure 3 is

$$J = J_m + J_g + \frac{J_a}{N^2}\,, \tag{12}$$

where J_a/N^2 is the "reflected" inertia of the ball screw axis drive, as seen by the motor through the gearbox. Similarly, B is the effective viscous damping, with contributions B_m, B_g, and B_a from the motor, gear system, and the ball screw axis drive. The block diagram in Figure 3 then yields

$$x(s) = \left[F(s) \cdot k_a \cdot k_t \cdot \frac{1}{Js + B} \cdot G(s) \cdot \frac{1}{s} \cdot r\right](X(s) - x(s))\,,$$

and for a P controller with $F(s) = k_p$ the closed–loop transfer function is

$$\frac{x(s)}{X(s)} = \frac{KH(s)}{KH(s) + (Js + B)s}\,, \tag{13}$$

where $K = k_p k_a k_t r/N$.

3.3 Governing differential equations

In general, the backlash transfer function $H(s)$ in (13) precludes closed–form inversion of the Laplace transform $x(s)$ of the output motion for a prescribed commanded motion, and the equations of motion must be integrated in the time domain, with appropriate "switching" between the backlash and non–backlash phases of the motion. The equations of motion, together with their appropriate initial conditions, are now formulated.

During each backlash interval $t \in [\, t_i, t_i + \Delta t_i \,]$ the ball screw axis drive is decoupled from the motor/gear system, and with no applied torque exhibits a "freewheeling" open–loop motion governed by its inertia J_a and damping B_a through the equation

$$J_a \frac{\mathrm{d}\omega}{\mathrm{d}t} + B_a\, \omega \;=\; 0\,.$$

With initial value $\omega(t_i)$ and setting $\alpha = B_a/J_a$, this has the solution

$$\omega(t) \;=\; \omega(t_i) \exp(-\alpha\,(t - t_i))\,, \quad t \in [\, t_i, t_i + \Delta t_i \,]\,.$$

Since $\omega(t) = \omega_m(t)/N$ during the prior non–backlash phase, with $\omega_m(t_i) = 0$ at the beginning of the backlash interval, then $\omega(t) \equiv 0$, $t \in [\, t_i, t_i + \Delta t_i \,]$. Consequently, the gearbox output shaft maintains a constant angular position $\theta_i = \theta(t_i)$, and the axis maintains the constant position $x_i = x(t_i)$ during the backlash phase. The x–axis position and velocity at the end of the backlash interval are therefore

$$x(t_i + \Delta t_i) \;=\; x_i \quad \text{and} \quad \dot{x}(t_i + \Delta t_i) \;=\; 0\,. \tag{14}$$

During the non–backlash interval $[\, t_i + \Delta t_i, t_{i+1} \,]$ the feedback loop remains closed, and there is full transfer of the amplified motor torque $N\,T_m$ to the ball screw axis drive. The x–axis position for a given commanded motion $X(t)$ is then governed by equation (8), subject to the initial conditions (14). Integrating this equation over $t \in [\, t_i + \Delta t_i, t_{i+1} \,]$ yields the initial conditions $x(t_{i+1}), \dot{x}(t_{i+1})$ for the backlash interval $[\, t_{i+1}, t_{i+1} + \Delta t_{i+1} \,]$. By considering a sequence of intervals with and without backlash in the above manner, the actual motion $x(t)$ for any given commanded motion $X(t)$ can be obtained.

3.4 Determination of backlash intervals

In general, the instances t_i at which the backlash phases commence and their durations Δt_i are not known *a priori*, and must be determined in real time.

A reasonable assumption is that backlash corresponds to a stationary output shaft of the gear system during a finite rotation $\Delta\theta_m > 0$ of the motor shaft, upon each reversal of the motor angular speed ω_m ($\Delta\theta_m$ is assumed to be the same for each reversal, and independent of the sense of each reversal). The backlash interval Δt_i is thus determined by the condition

$$\int_{t_i}^{t_i+\Delta t_i} \omega_m(t)\,\mathrm{d}t \;=\; \sigma\,\Delta\theta_m\,, \tag{15}$$

where σ is $+1$ or -1 according to whether ω_m changes negative to positive or positive to negative at $t = t_i$. During the backlash interval $[\,t_i, t_i + \Delta t_i\,]$ the motor is disconnected from the ball screw axis drive, so the axis maintains a fixed position $x_i = x(t_i)$ while the commanded position $X(t)$ may be varying.

From Figure 3, the transfer function relating the motor angular speed to the axis position error is

$$\frac{\omega_m(s)}{X(s) - x_i} \;=\; \frac{k_a k_t F(s)}{J_m s + B_m}\,,$$

and in the case of a P controller with $F(s) = k_p$ the corresponding differential equation

$$\frac{\mathrm{d}\omega_m}{\mathrm{d}t} + \beta\,\omega_m \;=\; C\,[\,X(t) - x_i\,]\,, \tag{16}$$

where $J_m = \eta J$ with $0 < \eta < 1$ and

$$\beta \;=\; \frac{B_m}{J_m}\,, \quad C \;=\; \frac{k_p k_a k_t}{J_m} \;=\; \frac{N}{\eta r b}\,.$$

Then equation (16) has, with initial condition $\omega_m(t_i) = 0$, the solution

$$\omega_m(t) \;=\; C\,\mathrm{e}^{-\beta t}\int_{t_i}^{t} \mathrm{e}^{\beta t}\,[\,X(t) - x_i\,]\,\mathrm{d}t\,, \quad t \in [\,t_i, t_i + \Delta t_i\,]\,. \tag{17}$$

The coefficient β may be determined by measuring the motor slow–down rate from an initial speed $\omega_m(0) \neq 0$ when disconnected from the power source at $t = 0$, since $\omega_m(t) = \omega(0)\;\mathrm{e}^{-t/\tau}$ where $\tau = 1/\beta$. The constant C is expressed in terms of the known gear reduction ratio N and ball screw transmission ratio r, the coefficient b in (9) obtained from the system identification, and the fraction η that the motor contributes to the overall inertia (12).

The expression (17) can be substituted in (15) to determine the duration Δt_i of the backlash interval. Depending on the commanded motion $X(t)$, the

integral in (17) may or may not admit closed–form reduction. To facilitate its evaluation, $X(t)$ will be specified by a simple harmonic motion, corresponding to an approximation of the commanded path by its osculating circle at each path turning point, as described below.

4 Analysis of canonical test case

Consider a commanded path corresponding to simple harmonic motion about $x = 0$ with amplitude a and frequency Ω — namely,

$$X(t) \;=\; a\,\sin\Omega\,t\,, \tag{18}$$

with the initial conditions are $x(0) = 0$ and $\dot{x}(0) = \Omega\,a$. At the beginning of the backlash interval $[\,t_i, t_i + \Delta t_i\,]$ the gearbox output shaft will have angular velocity $\omega = 0$, and since no torque is transmitted during this interval, the x–axis maintains a constant position, $x(t) = x(t_i)$ for $t \in [\,t_i, t_i + \Delta t_i\,]$.

Setting $\Delta = c^2 - 4\,b$ and $t_s = t_i + \Delta t_i$, the solution to equation (8) during the non–backlash interval $[\,t_i + \Delta t_i, t_{i+1}\,]$ that corresponds to the commanded motion (18) is of the form

$$x(t) \;=\; \begin{cases} \mathrm{e}^{-\gamma(t-t_s)}\,[\,c_1\,\mathrm{e}^{\lambda(t-t_s)} + c_2\,\mathrm{e}^{-\lambda(t-t_s)}\,] - g(t)\,, & \Delta > 0 \\ \mathrm{e}^{-\gamma(t-t_s)}\,[\,c_1\sin\lambda(t-t_s) + c_2\cos\lambda(t-t_s)\,] - g(t)\,, & \Delta < 0 \end{cases} \tag{19}$$

where

$$g(t) \;:=\; a\,(p\sin\Omega\,t + q\cos\Omega\,t)\,, \tag{20}$$

$$\gamma = \frac{c}{2b}\,,\quad \lambda = \frac{\sqrt{|\Delta|}}{2b}\,,\quad (p,q) = \frac{(b\,\Omega^2 - 1, c\,\Omega)}{(b\,\Omega^2 - 1)^2 + (c\,\Omega)^2}\,,$$

and the integration constants c_1, c_2 are determined from the initial conditions $x(t_s) = x_i$ and $\dot{x}(t_s) = 0$ for the non–backlash interval as

$$c_1 \;=\; \frac{(\lambda+\gamma)(x_i + g(t_s)) + \dot{g}(t_s)}{2\lambda}\,,\quad c_2 \;=\; \frac{(\lambda-\gamma)(x_i + g(t_s)) - \dot{g}(t_s)}{2\lambda}\,,$$

for $\Delta > 0$, and

$$c_1 \;=\; \frac{\gamma\,(x_i + g(t_s)) + \dot{g}(t_s)}{\lambda}\,,\quad c_2 \;=\; x_i + g(t_s)\,,$$

for $\Delta < 0$. The corresponding axis velocities and accelerations are

$$\begin{aligned}
\dot{x}(t) &= \mathrm{e}^{-\gamma(t-t_s)}\,[\,(\lambda-\gamma)\,c_1\,\mathrm{e}^{\lambda(t-t_s)} - (\lambda+\gamma)\,c_2\,\mathrm{e}^{-\lambda(t-t_s)}\,] - \dot{g}(t)\,, \\
\dot{x}(t) &= \mathrm{e}^{-\gamma(t-t_s)}\,[\,(\lambda\,c_1 - \gamma\,c_2)\cos\lambda(t-t_s) - (\gamma\,c_1 + \lambda\,c_2)\sin\lambda(t-t_s)\,] - \dot{g}(t)\,,
\end{aligned}$$

and

$$\begin{aligned}
\ddot{x}(t) &= \mathrm{e}^{-\gamma(t-t_s)}\,[\,(\lambda-\gamma)^2\,c_1\,\mathrm{e}^{\lambda(t-t_s)} + (\lambda+\gamma)^2\,c_2\,\mathrm{e}^{-\lambda(t-t_s)}\,] - \ddot{g}(t)\,, \\
\ddot{x}(t) &= \mathrm{e}^{-\gamma(t-t_s)}\,[\,((\gamma^2-\lambda^2)\,c_2 - 2\,\lambda\gamma\,c_1)\cos\lambda(t-t_s) \\
&\qquad + ((\gamma^2-\lambda^2)\,c_1 + 2\,\lambda\gamma\,c_2)\sin\lambda(t-t_s)\,] - \ddot{g}(t)\,.
\end{aligned}$$

The derivatives of (20) appearing in the above expressions are

$$\dot{g}(t) = a\,\Omega\,(p\cos\Omega\,t - q\sin\Omega\,t)\,, \quad \ddot{g}(t) = -\,a\,\Omega^2\,(p\sin\Omega\,t + q\cos\Omega\,t)\,.$$

4.1 Computing the backlash intervals

The preceding results determine the backlash and non–backlash motions over the intervals $[\,t_i, t_i + \Delta t_i\,]$ and $[\,t_i + \Delta t_i, t_{i+1}\,]$ but the instances t_i at which the backlash phases commence, and their durations Δt_i, must be determined.

The end t_i of the non–backlash interval $[\,t_{i-1} + \Delta t_{i-1}, t_i\,]$ following the backlash interval $[\,t_{i-1}, t_{i-1} + \Delta t_{i-1}\,]$ may be identified as the least value of t greater than $t_{i-1} + \Delta t_{i-1}$ satisfying $\dot{x}(t) = 0$, with the appropriate expression for the axis velocity according to whether Δ is positive or negative. From a sufficiently close initial estimate $t_i^{(0)}$ a sequence of Newton iterations

$$t_i^{(k)} = t_i^{(k-1)} - \frac{\dot{x}(t_i^{(k-1)})}{\ddot{x}(t_i^{(k-1)})}\,, \qquad k = 1, 2, \ldots$$

can be used to determine t_i to machine precision. For the commanded motion (18), the time between axis reversals is $T = \pi/\Omega$, and when the actual motion does not deviate severely from (18) the initial value $t_i^{(0)} = t_{i-1} + 0.9\,T$ yields rapid convergence to t_i.

For the commanded motion (18), the integral in equation (17) admits a closed–form reduction, yielding the motor angular speed as

$$\omega_m(t) = C\left[\,\frac{a\cos(\Omega\,t_i + \phi)\,\mathrm{e}^{-\,\beta(t-t_i)}}{\sqrt{\beta^2+\Omega^2}} - \frac{a\cos(\Omega\,t + \phi)}{\sqrt{\beta^2+\Omega^2}} - \frac{x_i}{\beta}\,[\,1 - \mathrm{e}^{-\,\beta(t-t_i)}\,]\,\right],$$

where ϕ is defined by

$$(\sin\phi, \cos\phi) \;=\; \frac{(\beta, \Omega)}{\sqrt{\beta^2 + \Omega^2}}\,.$$

Substituting for $\omega_m(t)$ into (15) and simplifying yields the equation

$$Q(\Delta t_i) \;:=\; f(0) - f(\Delta t_i) - \sigma\,\Delta\theta_m \;=\; 0\,, \tag{21}$$

where

$$f(\Delta t_i) \;:=\; C\left[\frac{a\cos(\Omega\,t_i + \phi)\,\mathrm{e}^{-\beta\,\Delta t_i}}{\beta\sqrt{\beta^2 + \Omega^2}} + \frac{a\sin(\Omega(t_i + \Delta t_i) + \phi)}{\Omega\sqrt{\beta^2 + \Omega^2}} + \frac{x_i}{\beta}\,(t_i + \Delta t_i) + \frac{x_i}{\beta^2}\,\mathrm{e}^{-\,\beta\Delta t_i}\right]. \tag{22}$$

The condition (21) determining Δt_i must also be solved iteratively. To obtain a starting approximation, note that $Q(0) = -\,\sigma\,\Delta\theta_m$, $Q'(0) = 0$, and $Q''(0) = C(\sin\Omega\,t_i - x_i)$, so the lowest–order non–trivial power series expansion of (21) about $\Delta t_i = 0$ yields the initial estimate

$$\Delta t_i^{(0)} \;=\; \left[\frac{2\,\sigma\,\Delta\theta_m}{C\,(a\sin\Omega\,t_i - x_i)}\right]^{1/2},$$

where the sign σ must be chosen to ensure the square root of a positive value. This initial estimate can be refined through a sequence of Newton iterations applied to (21). Note, however, that since (21) has a small derivative in the vicinity of $\Delta t_i = 0$, the convergence is relatively slow.

4.2 Illustrative example

The illustrative set of parameter values $b = 0.0005$ s^2, $c = 0.005$ s are chosen (so that $\Delta = -\,0.001975$ s), $N = 25$, $\eta = 0.35$, $r = 1.0$ m/rad, $\tau = 1/\beta = 1$ s, and $\Delta\theta_m = 0.125664$ rad. The commanded motion (18) has the amplitude $a = 0.25$ m and an interval $T = 6$ s between reversals, corresponding to the frequency $\Omega = \pi/T = 0.523599$ rad/s. These values are chosen to ensure that the influence of the gear backlash is clearly apparent. The derived parameters in Section 4 are $\gamma = 5$ s^{-1}, $\lambda = 44.440972$ s^{-1}, $C = 1.428571 \times 10^5$ rad/ms^2, $p = -\,1.000130$, $q = 0.002619$, and $\phi = 1.088448$ rad.

The motion starts with the initial conditions $x = 0$ and $\dot{x} = a\,\Omega$ at $t = 0$, and after a brief transient phase it settles down to a repetitive behavior with period $2\,T = 12$ s and a lag of 0.005001 s relative to the commanded motion. Each reversal is characterized by the backlash time interval $\Delta t_i = 0.118743$ s. Figure 5 illustrates the time variation of the x–axis position in the vicinity of an axis reversal. The position remains constant during the backlash interval Δt_i, and thereafter the controller attempts to restore the commanded motion. The oscillatory nature of this recovery reflects the underdamped nature of the system dynamics, characterized by the negative value of the quantity Δ.

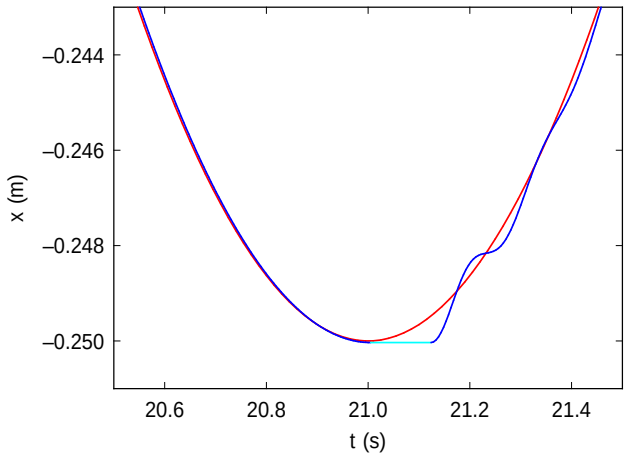

Figure 5: Representative output motion (blue & cyan) in response to backlash at an extreme point of the commanded motion (red) defined by (18) — the blue and cyan plots identify non–backlash and backlash phases of the motion.

For the circular motion $(X(t), Y(t)) = (a \sin \Omega\, t, a \cos \Omega\, t)$, with the same physical parameters for the x and y axes, Figure 6 compares the commanded and executed paths in the neighborhood of an x–axis turning point, with the discrepancy $\rho - a$ of the radial distance $\rho = \sqrt{x^2 + y^2}$ of the executed path from the origin amplified by the factor 25×.

5 Feedrate modulation scheme

Backlash compensation via part program modification may involve modifying the commanded path geometry or path speed (feedrate), or a combination of both. Feedrate modulation has been used to suppress variations in machining

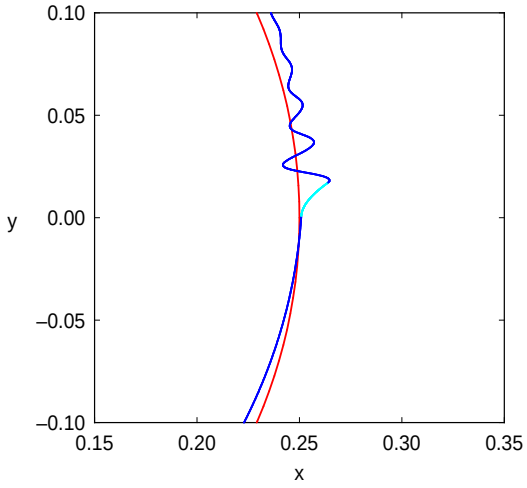

Figure 6: Commanded (red) and executed (blue/cyan) paths at an x–axis turning point for the circular motion $(X(t), Y(t)) = (a \sin \Omega\, t, a \cos \Omega\, t)$, with the radial distance error of the executed path magnified by the factor $25\times$.

forces [7], and path geometry modifications can minimize contour errors in high–speed execution of sharp path corners [12, 13].

Since determining the optimum modification parameters for the general case can be rather involved, the focus at present is on feedrate modulation and path modifications are deferred to a future study. Feedrate modulation for backlash compensation has been proposed by Warnecke and Jouaneh [23], using a piecewise–linear feedrate profile (which incurs discontinuities of the acceleration), determined from the backlash model developed in [11]. The approach adopted herein is based on feedrate profiles with a polynomial time dependence, which ensures continuity of both acceleration and jerk (time derivative of acceleration). Furthermore, for paths specified by Pythagorean–hodograph (PH) curves [5], such feedrate variations can be realized by simple and essentially exact real–time interpolator algorithms [22].

During a backlash interval, one axis remains stationary as the orthogonal axis continues to move with an (initial) speed equal to the feedrate V. The backlash position error therefore diminishes as the feedrate is V decreased. This is evident from Figure 7, based on the results of the analytic model in Section 4 for increasing times T between reversals of a single axis. This plot shows the distance traversed by the second axis while the first axis remains stationary as the gear system takes up the backlash — note that the feedrate

is $V = \pi a/T$, so increasing T corresponds to decreasing V.

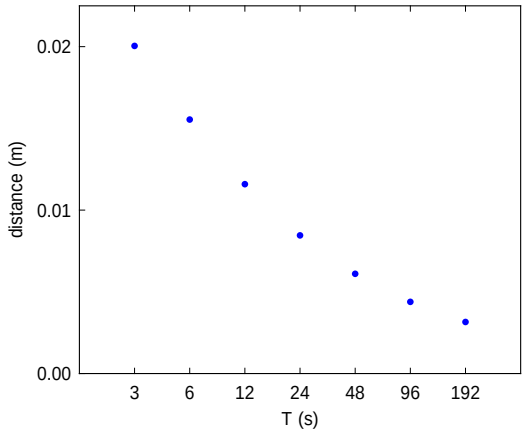

Figure 7: Variation of the distance travelled by the orthogonal axis while one axis remains stationary due to backlash, as a function of the time interval T between reversals of a single axis, based on the analytical model of Section 4.

Since it is impractical to run extended paths at very low feedrates, the approach adopted here is to employ smooth "local" feedrate reductions within small path segments that encompass each turning point. Although backlash begins at a turning point, feedrate suppression should commence beforehand to be most effective. The feedrate modulation is therefore implemented over a small path segments symmetric about the turning points.

Let $\mathbf{r}(\xi_0) = (x_0, y_0)$ be a vertical turning point with curvature $\kappa_0 \neq 0$ on a smooth free–form path $\mathbf{r}(\xi)$. It is convenient to take time $t = 0$ to be the instant at which the commanded path goes through the turning point $\mathbf{r}(\xi_0)$, identified by $\theta = 0$ on the osculating circle. Coordinates with origin at the point $\mathbf{r}(\xi_0)$ are employed, and path arc length is defined such that $s = 0$ at $\mathbf{r}(\xi_0)$. A path segment $s \in [\,-s_*, s_*\,]$ may then be approximated by the arc

$$x(\theta) \;=\; \rho_0(\cos\theta - 1)\,, \quad y(\theta) \;=\; \rho_0 \sin\theta\,, \quad \theta \in [\,-\theta_*, \theta_*\,] \tag{23}$$

of the osculating circle at $\mathbf{r}(\xi_0)$, where $\rho_0 = 1/\kappa_0$ is the radius of curvature and $\theta_* = s_*/\rho_0$.

5.1 Modulated feedrate function

Let $t \in [\,-t_*, t_*\,]$ be the time interval over which the feedrate is to be reduced. A normalized time variable

$$\tau \;=\; \frac{t + t_*}{2\,t_*}\,, \tag{24}$$

is introduced, such that $t \in [\,-t_*, t_*\,]$ is mapped to $\tau \in [\,0, 1\,]$ and derivatives with respect to t and τ are related by

$$\frac{\mathrm{d}}{\mathrm{d}t} \;=\; \frac{1}{2\,t_*}\frac{\mathrm{d}}{\mathrm{d}\tau}\,. \tag{25}$$

A time–dependent feedrate[2] will be employed, specified by a polynomial of even degree n in the time variable (24), represented in Bernstein form as

$$V(\tau) \;=\; \sum_{k=0}^{n} V_k \binom{n}{k} (1-\tau)^{n-k}\tau^k\,. \tag{26}$$

Let V_c be the nominal constant feedrate for $t < -\,t_*$ and $t > t_*$. For continuity of the velocity and acceleration at $t = -\,t_*$ and $t = t_*$, the coefficients of (26) must satisfy

$$V_0 \;=\; V_1 \;=\; V_c \;=\; V_{n-1} \;=\; V_n\,,$$

and consequently $n \geq 4$ if (26) is to incorporate free parameters that can be used to optimally suppress the influence of backlash.

Figure 8 shows examples of the feedrate function (26) of degree $n = 4$ and $n = 10$, with all the coefficients in (26) equal to V_c, except that $V_{n/2}$ is some multiple f of V_c. Hence $V(\tau)$ is symmetric about (and attains its extremum value at) $\tau = \frac{1}{2}$. Namely $V(\frac{1}{2}) = (5 + 3f)V_c/8$ and $(193 + 63f)V_c/256$ for $n = 4$ and $n = 10$, respectively (where $f > -5/3$ and $f > -193/63$ in these two cases, to ensure that V always remains positive). As evident in Figure 8, larger degrees n provide higher orders of continuity of the modulated feedrate (26) with the constant value V_c when $t < -\,t_*$ and $t > t_*$.

The arc–length interval $s \in [\,-s_*, s_*\,]$ on the osculating circle over which the reduced feedrate (26) holds can be determined by integrating $\mathrm{d}s/\mathrm{d}t = V$ to obtain

$$\int_{-s_*}^{s_*} \mathrm{d}s \;=\; \int_{-t_*}^{t_*} V(t)\;\mathrm{d}t \;=\; 2\,t_* \int_0^1 V(\tau)\;\mathrm{d}\tau\,,$$

[2] Analogous feedrate modulation functions have previously been used [8, 15] in the context of high–speed cornering motions.

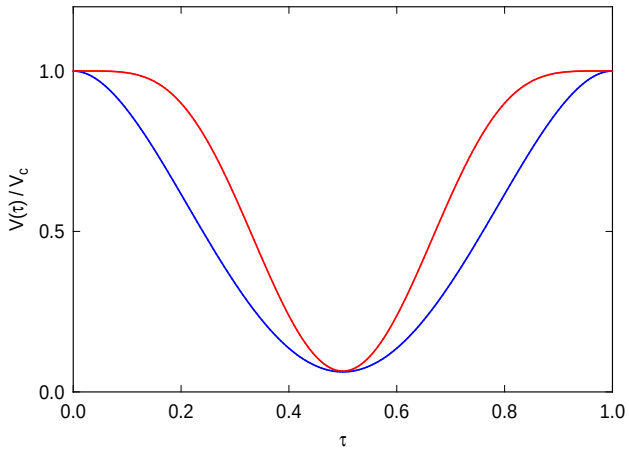

Figure 8: The feedrate modulation function defined by (26) with values (a) $n = 4$ with $V_0 = V_1 = V_c = V_3 = V_4$ and $V_2 = -1.5\,V_c$ (blue curve); and (b) $n = 10$ with $V_0 = \cdots = V_4 = V_c = V_6 = \cdots = V_{10}$, $V_5 = -\,2.8\,V_c$ (red curve).

and using the fact that the integral of a degree n Bernstein–form polynomial over $[\,0, 1\,]$ is simply [6] the sum of its coefficients divided by $n + 1$ yields

$$s_* \;=\; \frac{(V_0 + \cdots + V_n)\,t_*}{n+1}\,, \tag{27}$$

and this relation may be used to choose t_* so that the osculating circle does not deviate from the exact path by more than a desired tolerance ϵ over the segment $s \in [\,-s_*, s_*\,]$ on the osculating circle. The corresponding angular extent on the osculating circle is determined from $\theta_* = s_*/\rho_0$.

Note that, if the coefficient $V_{n/2}$ in (26) is set equal to $f\,V_c$ and all other coefficients are set equal to V_c, the time $2\,t_*$ required to traverse the segment $[\,-\,s_*, s_*\,]$ using (26) exceeds the traversal time $2\,s_*/V_c$ for a constant feedrate V_c by the relatively modest factor $(n+1)/(n+f)$.

5.2 Commanded motion

Consider motion on an extended portion $\theta \in [\,-\,\Theta_*, \Theta_*\,]$ of the osculating circle, with $\Theta_* > \theta_*$, corresponding to a time interval $t \in [\,-T_*, T_*\,]$. For $\theta \in [\,-\,\Theta_*, -\,\theta_*\,]$ and $\theta \in [\,\theta_*, \Theta_*\,]$ the motion is at a constant feedrate $\mathrm{d}s/\mathrm{d}t = V_c$, but for $\theta \in [\,-\,\theta_*, \theta_*\,]$ the feedrate function (26) is imposed.

The purpose of the "lead–in" and "lead–out" segments $\theta \in [\,-\Theta_*, -\theta_*\,]$ and $\theta \in [\,\theta_*, \Theta_*\,]$ is to minimize the influence of transient effects during the interval $\theta \in [\,-\theta_*, \theta_*\,]$ over which the modified feedrate is employed. The total time required for traversal of the extended osculating circle segment $[\,-\Theta_*, \Theta_*\,]$ is $2\,T_*$, where

$$T_* \;=\; t_* + \frac{\rho_0(\Theta_* - \theta_*)}{V_c}\,.$$

The duration of the motion is $t \in [\,-T_*, T_*\,]$. During the lead–in and lead–out phases, the commanded angular position $\Theta(t)$ increases at the constant rate $\Omega = V_c/\rho$. During the interval $t \in [\,-t_*, t_*\,]$ with the reduced feedrate (26), the commanded angular position is

$$\Theta(t) \;=\; -\,\theta_* + \int_{-t_*}^{t} \frac{V(t)}{\rho_0}\,\mathrm{d}t \;=\; -\,\theta_* + 2\,t_* \int_0^{\tau} \frac{V(\tau)}{\rho_0}\,\mathrm{d}\tau\,.$$

Now the degree $n+1$ polynomial defined by

$$S(\tau) \;=\; \int V(\tau)\,\mathrm{d}\tau \;=\; \sum_{k=0}^{n+1} S_k \binom{n+1}{k} (1-\tau)^{n-k}\tau^k \tag{28}$$

has [6] the Bernstein coefficients

$$S_0 \;=\; 0 \quad \text{and} \quad S_k \;=\; \frac{1}{n+1}\sum_{j=0}^{k-1} V_j\,, \quad k = 1, \ldots, n+1\,,$$

and hence the commanded angular position during the feedrate modulation phase can be expressed as

$$\Theta(t) \;=\; -\,\theta_* + \frac{2\,t_*}{\rho_0}\,S(\tau)\,, \tag{29}$$

where τ is defined in terms of t by (24). Referred to the turning point $\mathbf{r}(\xi_0)$ as origin, the commanded position is given in terms of $\Theta(t)$ by

$$X(t) \;=\; \rho_0\,[\,\cos\Theta(t) - 1\,]\,, \quad Y(t) \;=\; \rho_0 \sin\Theta(t)\,. \tag{30}$$

5.3 Equations of motion

For brevity, the x and y axes are assumed to be characterized by the same values for the constants (9). For the lead–in/out segments $[\,-\Theta_*, -\theta_*\,]$ and $[\,\theta_*, \Theta_*\,]$ executed at the constant feedrate V_c, the equations of motion for the x and y axes are then

$$b\,\ddot{x} + c\,\dot{x} + x = X\,, \quad b\,\ddot{y} + c\,\dot{y} + y = Y\,, \tag{31}$$

with commanded positions $X(t), Y(t)$ defined by (30). The initial conditions for the lead–in segment are then $(x(-T_*), y(-T_*)) = \rho_0(1 - \cos\Theta_*, -\sin\Theta_*)$ and $(\dot{x}(-T_*), \dot{y}(-T_*)) = V_c(\sin\Theta_*, \cos\Theta_*)$.

For the interval $t \in [\,-t_*, 0\,]$ the equations of motion (31) still hold, but the inputs correspond to the modulated feedrate defined by (24) and (26), and are specified by (29) and (30). However, the interval $[\,0, \theta_*\,]$ — during which the x–axis backlash occurs — must be treated differently.

During the backlash interval $t \in [\,0, \Delta t\,]$ the x-axis maintains the constant position $x_i = x(0)$ at the end of the interval $t \in [\,-t_*, 0\,]$ while the y–axis position is given by the solution of (31) with initial conditions $y(0), \dot{y}(0)$. For the time–dependent feedrate (26), the duration Δt of the backlash interval is more difficult to determine than for the simple model of Section 4, due to the complicated nature of the commanded motion defined by (28)–(30).

Consequently, Δt is computed by formulating equation (16) as the system of first–order equations

$$\frac{\mathrm{d}\omega_m}{\mathrm{d}t} = C\,[\,X(t) - x_i\,] - \beta\,\omega_m(t)\,, \quad \frac{\mathrm{d}\theta_m}{\mathrm{d}t} = \omega_m(t)\,, \tag{32}$$

for the motor angular speed ω_m and position θ_m. With $\theta_m(0) = \omega_m(0) = 0$, these equations can be accurately integrated by standard solution schemes for linear ordinary differential equations, using a sufficiently small time step δt. The instant t at which $|\theta_m(t)| = \Delta\theta_m$ will then identify the backlash interval Δt. The Δt values, for various combinations of the parameters β and C, can be computed offline to reduce the real–time controller computational burden.

Typically, $t_* \geq \Delta t$ is used so the backlash is completely taken up by the end of the interval $[\,-t_*, t_*\,]$. If $\Delta t < t_*$, the motion during the remaining time interval $[\,\Delta t, t_*\,]$ will be governed by equations (31) where $X(t), Y(t)$ are defined by (30) with $\Theta(t) = \theta_* + V_c(t - t_*)/\rho_0$, and the initial conditions are determined at the conclusion of the backlash interval.

6 Simulation results

To investigate the performance of the feedrate modulation scheme proposed in Section 5, the model parameters employed in Section 4.2 are used together with an angular extent $\Theta_* = \frac{1}{2}\pi$ of the lead–in/out path segments, and a modulated feedrate specified by (26) with $n = 10$ and a duration $[\,-t_*, t_*\,]$ defined by $t_* = 0.5$ s. The coefficients of (26) are all set equal to $V_c = \rho_0\Omega$, except that $V_5 = f\,V_c$. The value of f required to obtain a prescribed ratio $V(\frac{1}{2})/V_c$ is defined by

$$f \;=\; \frac{256\,V(\frac{1}{2})/V_c - 193}{63}\,.$$

The equations of motion were integrated with a time–step $\delta t = 0.001$ s.

Figure 9 compares commanded and executed paths at a vertical turning point, under the influence of backlash, for three different values of $V(\frac{1}{2})/V_c$ (note that the radial position error in this plot employs a 25× magnification). When this ratio equals 1 (i.e., a constant commanded feedrate V_c is imposed) the backlash incurs a significant underdamped tracking error. For $V(\frac{1}{2})/V_c = 0.25$, corresponding to a 75% feedrate reduction at the turning point, there is a substantial reduction in the magnitude of the backlash–induced position error. Finally, for $V(\frac{1}{2})/V_c = -\,0.5$ a retrograde motion is observed, with the magnitude of the reversed feedrate reaching 50% of V_c, and the magnified backlash position error is barely noticeable at the scale of the plot.

Since it is difficult to discern the retrograde motion of the $V(\frac{1}{2})/V_c = -0.5$ case in Figure 9, a "close–up" view is provided in Figure 10 — the cusps of the executed path correspond to the instances of feedrate reversal.

Figure 11 illustrates the depedence on the ratio $V(\frac{1}{2})/V_c$ of the maximum and root–mean-square values of the fractional radial deviation $e = (r-\rho_0)/\rho_0$ of the executed path during the interval $t \in [\,-t_*, t_*\,]$ where r is the distance of the path from the center of the osculating circle, and ρ_0 is its radius. Note that values of this ratio less than 0 and great than 1 are also included in this plot. The latter correspond to speeding up (rather than slowing down) the feedrate, and evidently incur worse positional errors. The former induce a "retrogade motion" phase during $t \in [\,-t_*, t_*\,]$ — i.e., the forward motion slows to a stop, reverses direction for a while, and then slows to a stop again before resuming the original forward direction.

For feedrates that do not incur a retrograde motion, the positional errors exhibit a shallow minimum at $V(\frac{1}{2})/V_c \approx 0.25$, corresponding to a modest

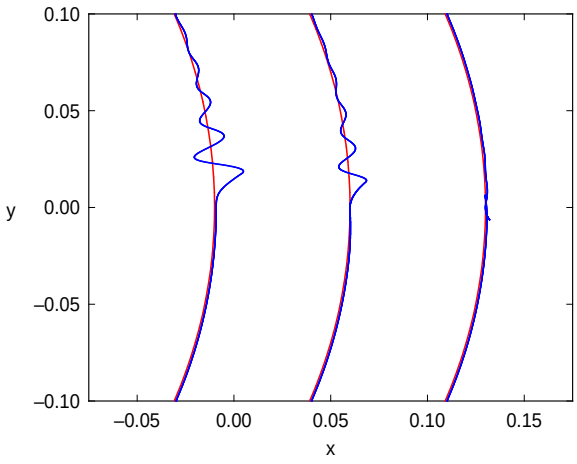

Figure 9: Commanded (red) and executed (blue) paths, with radial error for the executed path magnified 25×, for the feedrate function (26) specified by $n = 10$ and all coefficients equal to V_c except V_5, which is chosen such that the ratio $V(\frac{1}{2})/V_c$ corresponds to 1.0 (left); 0.25 (center); and -0.5 (right).

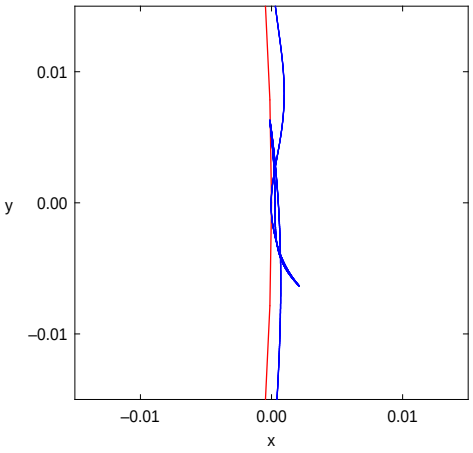

Figure 10: Close–up comparison of the commanded (red) and executed (blue) paths in the vicinity of the turning point, with radial error of the executed path magnified 25×, for the case $V(\frac{1}{2})/V_c = -0.5$ with a retrograde feedrate.

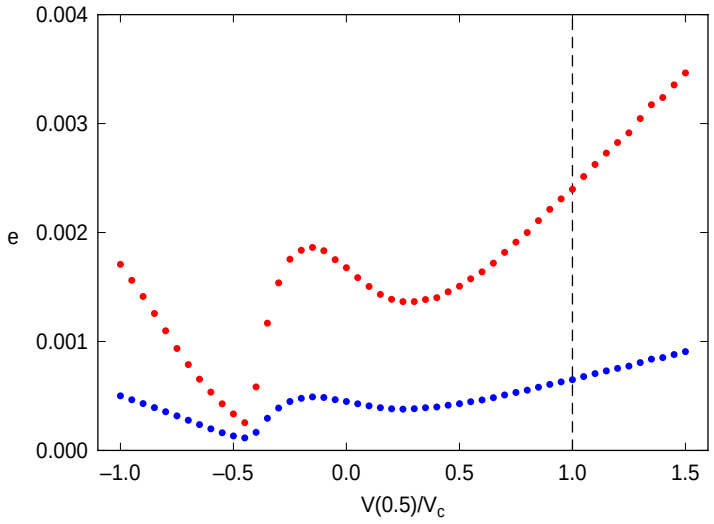

Figure 11: Variation of the maximum (red dots) and root–mean–square (blue dots) values for the fractional radial error of the executed motion during the feedrate modulation interval $t \in [\,-t_*, t_*\,]$, based on the feedrate modulation function specified by (26) with various values for the ratio $V(\frac{1}{2})/V_c$.

reduction compared to those for the constant feedrate V_c (identified by the dashed line in Figure 11). However, in the case of retrograde motion, a much more pronounced positional error reduction is evident at $V(\frac{1}{2})/V_c \approx -0.45$. This can be attributed to the fact that the "back–and–forth" motion arising from feedrate functions with $V(\frac{1}{2}) < 0$ essentially amounts to a dwell in the vicinity of the turning point, affording the motor shaft the spin–up time that is required to resolve the backlash of the gear system.

It might be thought that retrograde tool motion is undesirable in milling operations. Note, however, that it incurs no change of the commanded path geometry (subject to the tolerance of the osculating–circle approximation — see Section 2). In the case of a 2D milling operation with fixed depth of cut, for example, no additional material is removed during the retrograde phase. In other applications, such as 3D printing, it may be more problematic.

7 Closure

The key contributions of this study may be summarized as follows:

(1) the osculating circle path approximation was proposed, to facilitate the analysis of backlash at turning points of smooth analytic paths;

(2) a dynamic model for axis drive systems was developed, that can predict the onset and duration of backlash intervals;

(3) based on the dynamic model, a local feedrate modulation scheme was introduced to compensate for backlash positional errors;

(4) the efficacy of this scheme was demonstrated through simulations.

The backlash compensation scheme provides a simple means to improve the tracking accuracy of CNC machines without machine hardware or controller software upgrades. Results from an implementation of the methodology on an open–architecture CNC milling machine, including identification of optimum parameters, accuracy performance assessment, and a comparison with other approaches, will be presented in a forthcoming study.

For the case of a "dead–zone" backlash model and a simple P controller, the dynamic equations for backlash and non–backlash phases of the motion admit closed–form solutions, and the duration of the backlash phases can be determined by a simple iterative procedure. For a PI or PID controller, the solutions can be obtained through numerical integration.

The backlash compensation scheme is based on smooth suppression of the feedrate in a neighborhood of each path turning point. A significant feedrate reduction below the nominal value is found to substantially reduce backlash contour error at the turning points. Remarkably, suppressing the feedrate to negative values (which incurs a brief "retrograde" motion) is found to yield the maximum contour error reduction. This effectively provides a "dwell" at turning points, allowing the drive motor to resolve the axis backlash.

In contexts where retrograde motion is undesirable, significant reductions in contour error are still achievable through a choice of parameters that ensure non–negative feedrate. An alternative approach is to formulate a composite modulated feedrate function, consisting of a feed deceleration phase, a dwell phase at zero feedrate, and an acceleration phase back to the nominal feedrate value. These three phases should exhibit a high order of continuity at their junctures. A detailed description of this approach, together with the selection of appropriate parameters, is deferred to a future study.

The focus of this study has been on analysis and compensation of backlash positional errors incurred by the intrinsic machine dynamics. For machining

operations, the axis drive systems must also overcome cutting forces, and a detailed model of their variation for a given tool path and feedrate, depth and width of cut, workpiece specific cutting energy, etc., will be required to characterize and compensate for backlash contour errors. Since the feedrate modulation may require high localized axis accelerations, a further important issue in selecting the feedrate function parameters is the torque capacity of the drive motors. Investigation of these issues, and backlash compensation through path modification, will be pursued in subsequent studies.

References

[1] Y. Altintas (2000), *Manufacturing Automation: Metal Cutting Mechanics, Machine Tool Vibrations, and CNC Design*, Cambridge University Press.

[2] J.–J. Chou and D. C. H. Yang (1991), Command generation for three–axis CNC machining, *ASME J. Eng. Indus.* **113** 305–310.

[3] K. Erkorkmaz, C–H. Yeung, and Y. Altintas (2006), Virtual CNC system. Part II. High speed contouring application, *Int. J. Adv. Manuf. Technol.* **46**, 1124–1138.

[4] C. A. Ernesto and R. T. Farouki (2010), Solution of inverse dynamics problems for contour error minimization in CNC machines, *Int. J. Adv. Manuf. Technol.* **49**, 589–604.

[5] R. T. Farouki (2008), *Pythagorean–Hodograph Curves: Algebra and Geometry Inseparable*, Springer, Berlin.

[6] R. T. Farouki (2012), The Bernstein polynomial basis: a centennial retrospective, *Comput. Aided Geom. Design* **29**, 379–419.

[7] R. T. Farouki, J. Manjunathaiah, D. Nicholas, G.–F. Yuan, and S. Jee (1998), Variable feedrate CNC interpolators for constant material removal rates along Pythagorean–hodograph curves, *Comput. Aided Design* **30**, 631–640.

[8] R. T. Farouki and K. M. Nittler (2016), Efficient high–speed cornering motions based on continuously–variable feedrates I. Real–time interpolator algorithms, *Int. J. Adv. Manuf. Technol.* **87**, 3557–3568.

[9] R. T. Farouki and S. Shah (1996), Real–time CNC interpolators for Pythagorean–hodograph curves, *Comput. Aided Geom. Design* **13**, 583–600.

[10] R. T. Farouki and Y–F. Tsai (2001), Exact Taylor series coefficients for variable–feedrate CNC curve interpolators, *Comput. Aided Design* **33**, 155–165.

[11] P. Ge and M. Jouaneh (1998), Modeling of the backlash hysteresis nonlinearity, *J. Mech. Design* **120**, 408–413.

[12] B. M. Imani and J. Jahanpour (2008), High–speed contouring enhanced with PH curves, *Int. J. Adv. Manuf. Technol.* **37**, 747–759.

[13] J. Jahanpour and B. M. Imani (2008), Real–time PH curve CNC interpolators for high speed cornering, *Int. J. Adv. Manuf. Technol.* **39**, 302–316.

[14] R–S. Lin and Y. Koren (1996), Real–time interpolators for multi–axis CNC machine tools, *Manuf. Syst.* **25**, 145–149.

[15] K. M. Nittler and R. T. Farouki (2017), Efficient high–speed cornering motions based on continuously–variable feedrates II. Implementation and performance analysis, *Int. J. Adv. Manuf. Technol.* **88**, 159–174.

[16] M. Nordin and P. O. Gutman (2002), Controlling mechanical systems with backlash — a survey *Automatica* **38**, 1633–1649.

[17] T. F. Schraeder and R. T. Farouki (2014), Experimental performance analysis of an inverse dynamics CNC compensation scheme for high–speed execution of curved toolpaths, *Int. J. Adv. Manuf. Technol.* **73**, 195–208

[18] S. Shi, J. Lin, X. Wang, and X. Xu (2015), Analysis of the transient backlash error in CNC machines tools with closed loops, *Int. J. Mach. Tools Manuf.* **93**, 49–60.

[19] M. Shpitalni, Y. Koren, and C. C. Lo (1994), Realtime curve interpolators, *Comput. Aided Design* **26**, 832–838.

[20] D. J. Struik (1961), *Lectures on Classical Differential Geometry*, 2nd edition, Dover Publications, New York (reprint).

[21] Y. S. Tarng, Y. J. Kao, and Y. S. Lin (1997), Identification of and compensation for backlash on the contouring accuracy of CNC machining centres, *Int. J. Adv. Manuf. Technol.* **13**, 77–85.

[22] Y–F. Tsai, R. T. Farouki, and B. Feldman (2001), Performance analysis of CNC interpolators for time–dependent feedrates along PH curves, *Comput. Aided Geom. Design* **18**, 245–265.

[23] M. Warnecke and M. Jouaneh (2003), Backlash compensation in gear trains by means of open–loop modification of the input trajectory, *J. Mech. Design* **125**, 620–624.

[24] D. C. H. Yang and T. Kong (1994), Parametric interpolator versus linear interpolator for precision CNC machining, *Comput. Aided Design* **26**, 225–234.

[25] S–S. Yeh and P–L. Hsu (1999), The speed–controlled interpolator for machining parametric curves, *Comput. Aided Design* **31**, 349–357.

[26] C–H. Yeung, Y. Altintas, and K. Erkorkmaz (2006), Virtual CNC system. Part I. System architecture, *Int. J. Adv. Manuf. Technol.* **46**, 1107–1123.

Declarations

Funding

No funding was received in support of this research.

Conflicts of interest/Competing interests

The authors have incurred no conflicts of interest or competing interests in the conduct of this research.

Availability of data and material

No data or materials are available in connection with this research.

Code availability

There is no custom code or software available in connection with this research.

Authors' contributions

The authors have contributed equally in the conduct of this research.